

## Effect of positron–atom interactions on the annihilation gamma spectra of molecules

This article has been downloaded from IOPscience. Please scroll down to see the full text article.

2012 *New J. Phys.* 14 035021

(<http://iopscience.iop.org/1367-2630/14/3/035021>)

View the [table of contents for this issue](#), or go to the [journal homepage](#) for more

Download details:

IP Address: 132.239.1.231

The article was downloaded on 30/06/2012 at 02:22

Please note that [terms and conditions apply](#).

# New Journal of Physics

The open-access journal for physics

## Effect of positron–atom interactions on the annihilation gamma spectra of molecules

D G Green<sup>1,4</sup>, S Saha<sup>2</sup>, F Wang<sup>2</sup>, G F Gribakin<sup>1</sup> and C M Surko<sup>3</sup>

<sup>1</sup> Department of Applied Mathematics and Theoretical Physics,  
Queen's University Belfast, Belfast, BT71NN, UK

<sup>2</sup> Faculty of Life and Social Sciences, Swinburne University of Technology,  
Hawthorn, Victoria 3122, Australia

<sup>3</sup> Physics Department, University of California, San Diego, La Jolla,  
CA 92093-0319, USA

E-mail: [dermot.green@balliol.oxon.org](mailto:dermot.green@balliol.oxon.org)

*New Journal of Physics* **14** (2012) 035021 (26pp)

Received 17 January 2012

Published 28 March 2012

Online at <http://www.njp.org/>

doi:10.1088/1367-2630/14/3/035021

**Abstract.** Calculations of  $\gamma$ -spectra for positron annihilation on a selection of molecules, including methane and its fluoro-substitutes, ethane, propane, butane and benzene are presented. The annihilation  $\gamma$ -spectra characterise the momentum distribution of the electron–positron pair at the instant of annihilation. The contribution to the  $\gamma$ -spectra from individual molecular orbitals is obtained from electron momentum densities calculated using modern computational quantum chemistry density functional theory tools. The calculation, in its simplest form, effectively treats the low-energy (thermalised, room-temperature) positron as a plane wave and gives annihilation  $\gamma$ -spectra that are about 40% broader than experiment, although the main chemical trends are reproduced. We show that this effective ‘narrowing’ of the experimental spectra is due to the action of the molecular potential on the positron, chiefly, due to the positron repulsion from the nuclei. It leads to a suppression of the contribution of small positron-nuclear separations where the electron momentum is large. To investigate the effect of the nuclear repulsion, as well as that of short-range electron–positron and positron–molecule correlations, a linear combination of atomic orbital description of the molecular orbitals is employed. It facilitates the incorporation of correction factors which can be calculated from atomic many-body theory and account for the repulsion and correlations. Their inclusion in the

<sup>4</sup> Author to whom any correspondence should be addressed.

calculation gives  $\gamma$ -spectrum linewidths that are in much better agreement with experiment. Furthermore, it is shown that the effective distortion of the electron momentum density, when it is observed through positron annihilation  $\gamma$ -spectra, can be approximated by a relatively simple scaling factor.

## Contents

<b>1. Introduction</b>	<b>2</b>
<b>2. Theory: gamma-spectra for positron annihilation on molecules</b>	<b>4</b>
2.1. Basic equations . . . . .	4
2.2. The annihilation amplitude . . . . .	5
2.3. Direct annihilation rate from $\gamma$ -spectra . . . . .	7
<b>3. Gamma spectra from the density functional theory calculations</b>	<b>7</b>
<b>4. Effect of positron–atom interaction</b>	<b>9</b>
4.1. Electron momentum density: linear combination of atomic orbitals . . . . .	9
4.2. Atomic correction factors . . . . .	11
<b>5. Gamma spectra with atomic correction factors</b>	<b>14</b>
5.1. Molecular hydrogen . . . . .	14
5.2. Gamma spectrum of methane . . . . .	18
5.3. Gamma spectrum of tetrafluoromethane . . . . .	21
<b>6. Summary and conclusions</b>	<b>24</b>
<b>Acknowledgments</b>	<b>24</b>
<b>References</b>	<b>25</b>

## 1. Introduction

In the dominant positron annihilation process in matter, a positron annihilates with an electron to produce two gamma ( $\gamma$ ) photons with a total energy of  $2mc^2$  and a total momentum  $\mathbf{P}$  [1, 2]. Nonzero values of  $\mathbf{P}$  lead to Doppler shifts of the photon energies from  $mc^2 \approx 511\text{ keV}$ . In the case of bound electrons, this Doppler broadening is mostly due to the electron momenta [3–5]—the spectra of  $\gamma$ -ray energies (the ‘ $\gamma$ -spectra’) therefore contain information about the electron momentum distribution in the bound-state orbitals and can be used to characterize the orbitals involved [6–9].

In light of this fact, positron annihilation spectroscopy is a valuable technique in the study of surfaces, interfaces and defects in condensed matter [10, 11], of electronic properties of quantum dots [12–17], nanoparticles [18, 19] and nanocrystals [20], and in the study and exploitation of positron annihilation on core electrons [4, 8, 21–25].

In all of these areas, interpretation of the measured annihilation spectra relies heavily on theoretical input. However, the problem of calculating  $\gamma$ -spectra for positron annihilation on molecules has received little attention to date, with previous positron–molecule theoretical studies focused mainly on understanding the anomalously large annihilation rate parameters  $Z_{\text{eff}}$  [26]. This is in contrast with condensed matter systems, where a number of theoretical approaches have been developed [10, 11], and atomic systems, for which detailed theoretical understanding has been provided by, e.g. elaborate variational [5] and many-body theory [6–8] calculations. The aim of this paper is to present calculations of  $\gamma$ -spectra for positron

annihilation on a range of molecules including hydrogen, methane and its fluoro-substitutes, ethane, propane, butane and benzene.

The first measurement of the Doppler-broadened  $\gamma$ -spectrum for positron annihilation on molecules was made in 1986 by Brown and Leventhal in low-density hydrogen gas [27]. In the early 1990s the confinement of thermalized positrons in a Penning trap allowed Tang *et al* [28] to measure  $\gamma$ -spectra for a range of molecules, including hydrocarbons and perfluorocarbons. This work was built upon by Iwata *et al* [3] who measured  $\gamma$ -spectra for positron annihilation on a large range of atoms and molecules in the gas phase. Despite this extensive set of experimental results, there is a paucity of theoretical calculations of the annihilation  $\gamma$ -spectra in molecules. Theoretical predictions of the  $\gamma$ -spectra do exist for the molecular ion  $H_2^+$ , for which (numerical) Coulomb–Born and configuration–interaction Kohn variational calculations have been performed [29], and for the small molecules  $H_2$  and  $N_2$  [30, 31]. However, the application of these sophisticated methods to larger molecules is considerably more difficult. More than thirty years ago Chuang and Hogg [32] analysed the annihilation  $\gamma$ -spectra for hexane and decane. However, their calculation for the alkane molecules relied on analytic wave functions of the carbon orbitals calculated in the 1950s, which are relatively crude by modern standards. Furthermore, their calculations disregarded the effect of the positron wavefunction. New calculations using modern quantum chemistry methods, similar to those reported here, are underway [33].

Although the  $\gamma$ -spectra are determined primarily by the electronic structure, they are also sensitive to the positron interaction with the target. Compared to positron annihilation on atoms, the positron–molecule problem is significantly more complex owing to, e.g. the non-spherical potential experienced by the positron. In this work we use two methods to calculate  $\gamma$ -spectra for positron annihilation on molecules. The first method is based on electron momentum densities calculated from modern computational chemistry tools, such as density functional theory (DFT). This approach was recently tested by a number of the authors in a study of positron annihilation on noble gases [9] and applied to fluorobenzenes [33]. In its simplest form, this method treats the positron as a plane wave and neglects its influence on the  $\gamma$ -spectrum linewidth. To overcome this deficiency, and to investigate the effect of the atomic potentials and electron–positron correlations, we perform additional calculations that rely on treating the molecular orbitals as linear combinations of atomic orbitals. This yields predicted spectra that are in good agreement with the computational chemistry calculations and furthermore, it gives a framework for the inclusion of the effect of the atomic potentials and correlations on the  $\gamma$ -spectrum linewidth (see [34] for preliminary results).

The structure of the paper is as follows. Section 2 briefly recaps the general theory of positron annihilation  $\gamma$ -spectra. In section 3 the results of the DFT calculations are presented for molecular hydrogen, methane and its fluoro-substitutes, ethane, propane, butane and benzene. This DFT calculation effectively ignores the effect of the positron–molecule interaction on the  $\gamma$ -spectra, and gives  $\gamma$ -spectra that are systematically broader than experiment. In section 4 an investigation of the systematic broadening is performed. There, we derive the form of the annihilation  $\gamma$ -spectra for molecules using a multicentre linear combination of atomic orbital (LCAO) approach. We also show how, in this scheme, the effect of the nuclear repulsion and electron–positron correlations can be accounted for through momentum-dependent correction factors obtained from positron–atom calculations, e.g. using many-body theory. This procedure is applied to  $H_2$ ,  $CH_4$  and  $CF_4$  in section 5. In light of our results, we discuss how the effective distortion of the electron momentum density, when it is observed through positron annihilation

$\gamma$ -spectra, can be approximated by a relatively simple energy scaling factor. We conclude with a summary in section 6.

## 2. Theory: gamma-spectra for positron annihilation on molecules

### 2.1. Basic equations

Low-energy positrons annihilate in matter predominately via two-photon production, a process in which the total spin of the electron–positron pair must be zero [2, 35]. In the centre-of-mass frame of the pair, where the total momentum of the two photons  $\mathbf{P} = \mathbf{p}_{\gamma_1} + \mathbf{p}_{\gamma_2}$  is zero, the two photons propagate in opposite directions and have equal energies  $E_\gamma = p_\gamma c = mc^2 + \frac{1}{2}(E_i - E_f) \approx mc^2 = 511 \text{ keV}$ , where  $E_i$  and  $E_f$  are the energies of the initial and final states (excluding rest mass), respectively. When  $\mathbf{P}$  is nonzero, however, the two photons no longer propagate in exactly opposite directions and their energies are Doppler shifted. For example, for the first photon  $E_{\gamma_1} = E_\gamma + m\mathbf{c} \cdot \mathbf{V}$ , where  $\mathbf{V} = \mathbf{P}/2m$  is the centre of mass velocity of the electron-positron pair and  $\mathbf{c} = c\hat{\mathbf{c}}$ , where  $\hat{\mathbf{c}}$  is the unit vector in the direction of the photon. Assuming that  $V \ll c$ , and  $p_{\gamma_1} = E_{\gamma_1}/c \approx mc$ , the shift of the photon energy from the centre of the line,  $\epsilon \equiv E_{\gamma_1} - E_\gamma$ , is

$$\epsilon = m\mathbf{c} \cdot \mathbf{V} = \frac{1}{2}\mathbf{P} \cdot \mathbf{c}. \quad (1)$$

When a low-energy positron annihilates with a bound electron, the characteristic Doppler shifts are determined by the electron energy  $\varepsilon_n$ ,  $\epsilon \sim \sqrt{|\varepsilon_n|mc^2} \gg |\varepsilon_n|$ . Hence, the shift of the line centre  $E_\gamma$  from  $mc^2 = 511 \text{ keV}$  can usually be neglected. The annihilation  $\gamma$ -spectrum (Doppler spectrum) can then be written in a form similar to a Compton profile, as the integral of the annihilation probability density

$$w_{fi}(\epsilon, \hat{\mathbf{c}}) = \int |A_{fi}(\mathbf{P})|^2 \delta\left(\epsilon - \frac{1}{2}\mathbf{P} \cdot \mathbf{c}\right) \frac{d^3 P}{(2\pi)^3}, \quad (2)$$

where  $A_{fi}(\mathbf{P})$  is the amplitude for annihilation into two photons. It is the fundamental quantity to be evaluated. A many-body theory description of it is discussed below.

For gaseous systems, the measured spectrum represents an average of  $w_{fi}(\epsilon, \hat{\mathbf{c}})$  over the direction of emission of the annihilation photons [6, 8]

$$w_{fi}(\epsilon) = \frac{1}{c} \int_{2|\epsilon|/c}^{\infty} \rho_{fi}^a(P) 4\pi P dP, \quad (3)$$

where

$$\rho_{fi}^a(P) \equiv \int \frac{|A_{fi}(\mathbf{P})|^2}{(2\pi)^3} \frac{d\Omega_{\mathbf{P}}}{4\pi}, \quad (4)$$

is the spherically averaged annihilation momentum density. If the initial state corresponds to a positron with momentum  $\mathbf{k}$  incident on the ground-state target, and the possible final states describe the target with an electron missing in orbital  $n$ , the total spectrum is found by summing over all final states as

$$w_{\mathbf{k}}(\epsilon) = \sum_n w_{n\mathbf{k}}(\epsilon) = \frac{1}{c} \int_{2|\epsilon|/c}^{\infty} \rho_{\mathbf{k}}^a(P) 4\pi P dP, \quad (5)$$

where  $\rho_{\mathbf{k}}^a(P) = \sum_n \rho_{n\mathbf{k}}^a(P)$  is the total annihilation momentum density that is equal to the sum of the individual annihilation momentum densities of the occupied molecular orbitals  $n$ . The

probability of positron annihilation with core electrons is relatively small (owing to the positron repulsion from the nuclei). Hence, the annihilation spectra are dominated by the contribution of valence orbitals, except at high Doppler shifts where a distinct contribution from the core can be seen [4, 8].

## 2.2. The annihilation amplitude

### 2.2.1. General form.

The annihilation amplitude that enters (3) is defined as

$$A_{n\mathbf{k}}(\mathbf{P}) = \left\langle \Psi_n^{N-1} \left| \int e^{-i\mathbf{P}\cdot\mathbf{r}} \hat{\psi}(\mathbf{r}) \hat{\phi}(\mathbf{r}) d^3r \right| \Psi_{\mathbf{k}}^{N+1} \right\rangle, \quad (6)$$

where  $\hat{\psi}(\mathbf{r})$  and  $\hat{\phi}(\mathbf{r})$  are the electron and positron annihilation operators, respectively,  $\Psi_{\mathbf{k}}^{N+1}$  is the (fully-correlated) initial state of  $N$  electrons and a positron of momentum  $\mathbf{k}$ , and  $\Psi_n^{N-1}$  is the (fully-correlated) final state of the target with  $N - 1$  electrons and a hole in electron orbital  $n$ . It can be calculated using many-body theory methods (see [6–8] for details).

Figure 1 shows the many-body diagrammatic expansion for the amplitude (see the figure caption for an explanation of the diagrams). More specifically, it shows the main contributions to the annihilation vertex that describes the short-range electron–positron interaction. Figure 1(a) is the zeroth-order, or independent-particle-model (IPM) amplitude, which is given by

$$A_{n\mathbf{k}}^{(0)}(\mathbf{P}) = \int e^{-i\mathbf{P}\cdot\mathbf{r}} \psi_n(\mathbf{r}) \varphi_{\mathbf{k}}(\mathbf{r}) d^3r, \quad (7)$$

where  $\varphi_{\mathbf{k}}$  is the wavefunction of the positron, and  $\psi_n$  is the wavefunction of the annihilated electron (hole) in state  $n$ . Figures 1(b) and (c) describe the short-range electron–positron correlation corrections to the zeroth-order vertex. Their explicit forms can be found in [6–8]. In addition to the short-range electron–positron correlations, there are also correlations between the incident positron and the target, e.g. through a polarization interaction. These interactions are described by a non-local and energy dependent positron self-energy [6–8, 36]. They are included in the fully-correlated (or ‘dressed’) incident positron wavefunction known as the *Dyson orbital*, which is represented by the double line labelled  $\varepsilon$  in figure 1.

When evaluating the diagrams beyond zeroth order, one must sum over the complete set of intermediate electron and positron wavefunctions, including those in the continuum. This summation can be performed relatively easily for atomic systems, since the spherical potential allows for the wavefunctions to be separated into radial and angular parts and asymptotic convergence formulae can be used [6–8, 36, 37]. However, the lack of spherical symmetry in the molecular problem makes the development of a numerical scheme in which the higher-order diagrams can be calculated a more difficult task.<sup>5</sup> Nevertheless, the shape of the  $\gamma$ -spectra is described to a good first approximation by the zeroth-order amplitude [4, 6–8], the calculation of which requires only accurate positron and electron wavefunctions. We will use this as our starting point.

To go beyond the zeroth-order approximation and incorporate the effects of the higher-order diagrams on the lineshape, we will assume that the positron annihilates in the vicinity of

<sup>5</sup> In evaluating the diagrams for a molecular system one would have to, e.g. transform the Hartree–Fock eigenbasis to a (non-orthogonal) one that involves (at least) the atomic orbitals that constitute the molecule, centred on their respective atomic sites, as is standard in the derivation of the Roothaan equations. Alternatively, one can use a Gaussian basis.

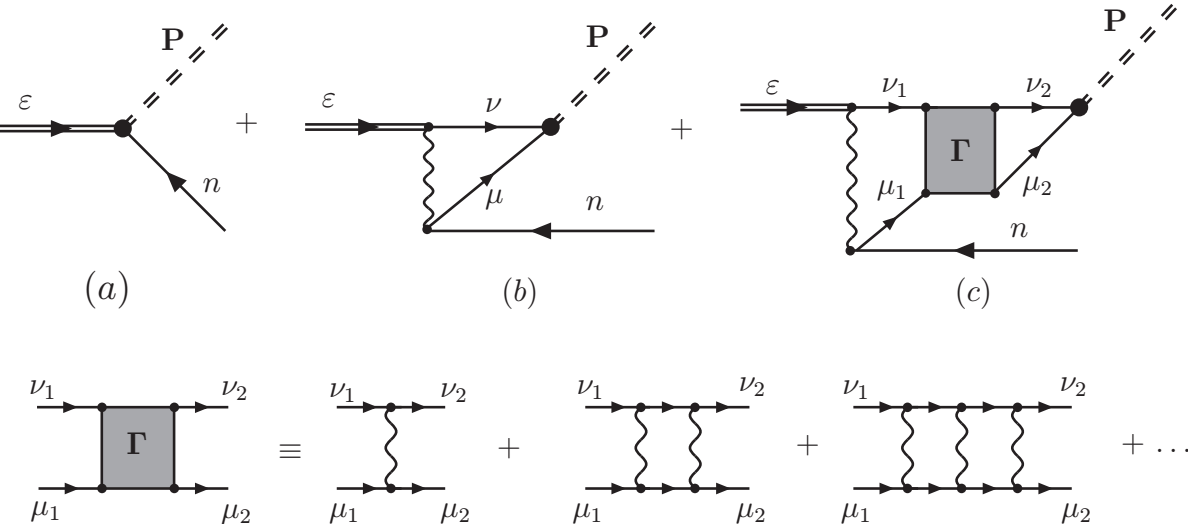


**Figure 1.** Main contributions to the annihilation amplitude  $A_{n\mathbf{k}}(\mathbf{P})$ : (a) zeroth-order (independent-particle model); (b) first-order correction; (c)  $\Gamma$ -block (electron–positron ladder series) correction. All lines correspond to particles (or holes) propagating on top of the ground state of the  $N$ -electron system. The fully-correlated incident positron wavefunction (Dyson orbital) is represented by the double line labelled  $\varepsilon$ ; the wavefunction of the annihilated electron (hole) is labelled by  $n$ ; the double-dashed lines represent the two photons of momentum  $\mathbf{P}$ ; wavy lines represent Coulomb interactions; and  $\nu$  and  $\mu$  are excited positron and electron states, respectively.

one of the atoms of the molecule. The annihilation amplitude diagrams can then be calculated using positron and electron orbitals in the field of the *atomic* potentials.

**2.2.2. Plane-wave positron, independent-particle approximation.** If one assumes that the positron is described by a plane wave, then in the low-energy limit  $k \ll 1 \text{ au}$ , one has  $\psi_{\mathbf{k}}(\mathbf{r}) = e^{i\mathbf{k}\cdot\mathbf{r}} \approx 1$ , for the range of distances at which annihilation occurs.<sup>6</sup> In this case the zeroth-order annihilation momentum density (equations (4) and (7)) reduces to

$$\rho_{n\mathbf{k}}^{a(0)}(P) \simeq \int |\tilde{\psi}_n(\mathbf{P})|^2 \frac{d\Omega_{\mathbf{p}}}{4\pi} \equiv \rho_n(P), \quad (8)$$

where

$$\tilde{\psi}_n(\mathbf{P}) = (2\pi)^{-3/2} \int e^{-i\mathbf{P}\cdot\mathbf{r}} \psi_n(\mathbf{r}) d^3r \quad (9)$$

is the momentum space wavefunction, and  $\rho_n$  is the spherically averaged electron momentum density of the orbital  $n$ .<sup>7</sup> The  $\gamma$ -spectrum (cf (5)) then takes the form

$$w(\epsilon) = \frac{1}{c} \int_{2|\epsilon|/c}^{\infty} \rho(P) 4\pi P dP, \quad (10)$$

<sup>6</sup> Annihilation occurs at distances of the size of the atom or molecule involved.

<sup>7</sup> The density is normalized by  $\int \rho_n(P) 4\pi P^2 dP = 1$ .

where  $\rho(P) = \sum_n \rho_n(P)$  is the total electron momentum density of the occupied orbitals in the molecule. It is related to the cross section measured using the electron-momentum spectroscopy technique [38].

### 2.3. Direct annihilation rate from $\gamma$ -spectra

The electron–positron direct annihilation rate in a gas of density  $n$  is commonly parameterized through the dimensionless quantity  $Z_{\text{eff}}$ , defined as the ratio of the observed annihilation rate  $\lambda$  to the rate of free electron-positron annihilation  $Z_{\text{eff}} \equiv \lambda/\pi r_0^2 cn$  [39, 40]. By definition,  $Z_{\text{eff}}$  quantifies the *effective number of electrons* per target atom or molecule, with which the positron can annihilate. In general, it is different from the true number of electrons  $Z$  owing to the effects of, e.g. the nuclear repulsion and positron–electron interactions, which can act to suppress or enhance the electron density in the vicinity of the positron. For most molecules,  $Z_{\text{eff}}$  is also enhanced by the vibrational Feshbach resonances [26]. The ratio  $Z_{\text{eff}}/Z$  therefore gives a measure of the strength of such effects.  $Z_{\text{eff}}$  can be calculated in terms of the Doppler spectrum, and hence annihilation momentum density, as

$$Z_{\text{eff}} = \int_{-\infty}^{\infty} w_{\mathbf{k}}(\epsilon) d\epsilon = \int_0^{\infty} \rho_{\mathbf{k}}^a(P) 4\pi P^2 dP. \quad (11)$$

For a plane-wave positron, in the independent-particle-model approximation, it reduces to  $Z_{\text{eff}} = Z$ , the number of electrons in the molecule.

## 3. Gamma spectra from the density functional theory calculations

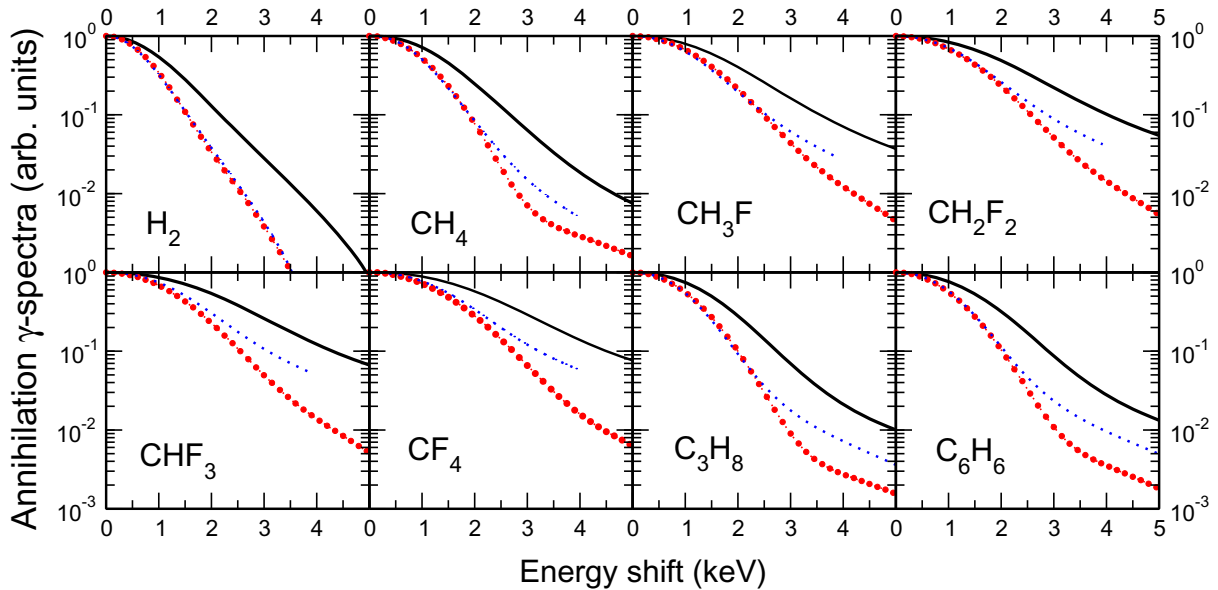
In this section we present the results of the calculations of the  $\gamma$ -spectra for a selection of molecules. They were performed assuming a plane-wave positron, and were based on electron-momentum distributions, equations (8)–(10). Specifically, we used the DFT-based Becke-3-parameter Lee–Yang–Parr (B3LYP) model [41, 42], with the Godbout polarised triple- $\zeta$  valence (TZVP) basis set [43], which is known to produce good agreement with the experimental measurements for the molecular orbital momentum profiles [44]. These calculations were performed using the computational chemistry package Gaussian 03 [45]. For C<sub>3</sub>H<sub>8</sub> and C<sub>6</sub>H<sub>6</sub> we used the BP86 functional in GAMESS [46]. The calculations employed finite cut-off momentum values in calculating the spectra from (10) (in most cases,  $P_{\text{max}} = 3$  au). When possible, tails of the form  $AP^{-\xi}$  were added to the orbital momentum densities to obtain more accurate spectra. In most cases this did not change their widths by more than 5%.

Figure 2 shows the results of our plane-wave-positron DFT calculation for the annihilation  $\gamma$ -spectra of hydrogen, the fluorosubstituted methanes, and propane and benzene. Also shown are the experimental results of Iwata *et al* [3] obtained assuming that the intrinsic annihilation line shapes can be described by the two-Gaussian form,

$$w(\epsilon) \propto \exp(-\epsilon^2/a^2) + A \exp(-\epsilon^2/b^2), \quad (12)$$

where  $A$ ,  $a$  and  $b$  are constants obtained by deconvoluting the intrinsic spectra from the measured line shapes. Their values for an extensive range of molecules can be found in [3].

The values of the calculated and measured full-widths at half-maximum (FWHM) are given in table 1. For all of the molecules studied, the calculation systematically overestimates the measured line widths, although the main chemical trends are reproduced. This can also be seen in figure 3, where we plot the calculated FWHM versus the measured linewidths for all of the



**Figure 2.** Annihilation  $\gamma$ -spectra for a selection of molecules: —, DFT calculation (neglecting the contributions of core orbitals, i.e. C 1s and F 1s); ·····, DFT spectra scaled as described at the end of section 5.1.1; ●, experiment (two-Gaussian fit) [3].

**Table 1.** Full widths at half-maximum (keV) of the calculated and measured  $\gamma$ -spectra for molecules.

	H <sub>2</sub>	CH <sub>4</sub>	CH <sub>3</sub> F	CH <sub>2</sub> F <sub>2</sub>	CHF <sub>3</sub>	CF <sub>4</sub>	C <sub>2</sub> H <sub>6</sub>	C <sub>3</sub> H <sub>8</sub>	C <sub>4</sub> H <sub>10</sub>	C <sub>6</sub> H <sub>6</sub>
DFT <sup>a</sup>	2.14	2.81	3.40	3.81	4.08	4.29	3.05	2.99	3.12	3.14
Experiment <sup>b</sup>	1.59	2.06	2.64	2.72	2.71	2.92	2.15	2.18	2.25	2.20

<sup>a</sup> B3LYP or BP86 calculation of the electron momentum density (i.e. the plane-wave positron approximation) without the tails. Core-electron contributions are omitted, except for C<sub>2</sub>H<sub>6</sub> and C<sub>4</sub>H<sub>10</sub>.

<sup>b</sup> Experimental values from the two-Gaussian fit of [3].

molecules discussed, and for the noble gases Ne, Ar, Kr and Xe that were calculated using the Hartree–Fock (HF) method [9].<sup>8</sup> The graph shows that the FWHM values from plane-wave positron approximation are greater than the experimental values by about 40%.

The main origin of the discrepancy between these calculations and experiment is the neglect of the effect of the positron–molecule potential, and in particular, the positron repulsion from the nuclei, in the calculation. It leads to an overestimate of the electron–positron wavefunction overlap at small positron–nuclear separations, and therefore, of the large momentum contributions to the annihilation momentum density and of the large energy shifts in the  $\gamma$ -spectra.

<sup>8</sup> Note that for the noble gas atoms, many-body theory calculations are much superior to the plane-wave-positron HF method shown here, and produce  $\gamma$ -spectra in excellent agreement with experiment [6, 8].

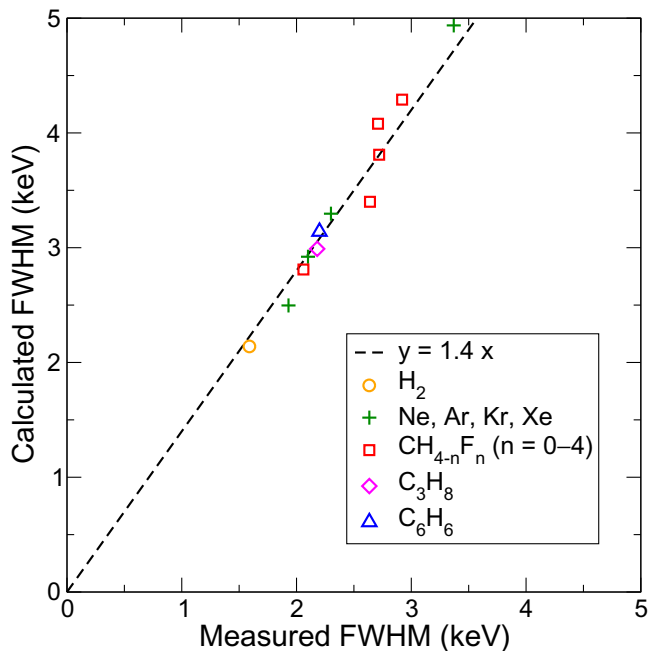


**Figure 3.** FWHM values of the  $\gamma$ -spectra calculated in the plane-wave-positron approximation versus experimental values from [3], for a range of molecules and noble-gas atoms. The dashed line is a linear relation  $y = 1.4x$ .

One should expect that the proper inclusion of the positron–nuclear repulsion will lead to a narrowing of the spectra, bringing them into better agreement with experiment. The remainder of the paper outlines a scheme which facilitates this inclusion.

#### 4. Effect of positron–atom interaction

##### 4.1. Electron momentum density: linear combination of atomic orbitals

To account for the effect of the nuclear repulsion and electron-positron correlations, it is instructive to derive the electron momentum density for a given molecular orbital using a multicentre LCAO. To do this we follow the approach of [47].

First, consider a generic molecular orbital  $\psi(\mathbf{r})$  as a linear combination of the atomic orbitals  $\psi_i$  that constitute the molecule,

$$\psi(\mathbf{r}) = \sum_i c_i \psi_i(\mathbf{r} - \mathbf{R}_i), \quad (13)$$

where  $c_i$  are the expansion coefficients,<sup>9</sup> and  $\mathbf{R}_i$  are the coordinates of the atomic centres.<sup>10</sup>

Assuming the atomic orbitals can be written in the central-field form  $\psi_{nlm}(\mathbf{r}) = R_{nl}(r)Y_{lm}(\hat{\mathbf{r}})$ , where  $R_{nl}$  is the radial function and  $Y_{lm}$  is a spherical harmonic, the corresponding

<sup>9</sup> In general the expansion coefficients are governed by the point-group symmetry of the molecule, and by requirements of normalization and energy minimization.

<sup>10</sup> In the Born–Oppenheimer approximation the set of the  $\mathbf{R}_i$  are external parameters as opposed to dynamical variables.

momentum space wavefunction (9) is

$$\tilde{\psi}_{nlm}(\mathbf{P}) = (-i)^l \tilde{R}_{nl}(P) Y_{lm}(\hat{\mathbf{P}}), \quad (14)$$

where  $\tilde{R}_{nl}(P) = \sqrt{\frac{2}{\pi}} \int_0^\infty j_l(Pr) R_{nl}(r) r^2 dr$ . The spherically averaged momentum density for this atomic orbital, equation (8), is then given by

$$\rho_{nl}(P) = \tilde{R}_{nl}^2(P)/4\pi. \quad (15)$$

Hence, the momentum-space wavefunction can then be written as

$$\tilde{\psi}_i(\mathbf{P}) = (-i)^{l_i} \sqrt{4\pi \rho_i(P)} Y_{l_i m_i}(\hat{\mathbf{P}}), \quad (16)$$

where  $i$  labels the specific atomic orbital in the linear combination (13) and implicitly includes the labels for the quantum numbers  $n$  and  $l$ . The momentum-space molecular orbital can then be expressed as follows:

$$\tilde{\psi}(\mathbf{P}) = (2\pi)^{-3/2} \int e^{-i\mathbf{P}\cdot\mathbf{r}} \psi(\mathbf{r}) d^3r, \quad (17)$$

$$= \sum_i c_i e^{-i\mathbf{P}\cdot\mathbf{R}_i} \tilde{\psi}_i(\mathbf{P}), \quad (18)$$

and the corresponding momentum density  $\rho(P)$  is easily shown to be

$$\rho(P) = \sum_{i,j} (-i)^{l_j - l_i} c_i^* c_j \sqrt{\rho_i(P) \rho_j(P)} \int e^{i\mathbf{P}\cdot(\mathbf{R}_i - \mathbf{R}_j)} Y_{l_i m_i}^*(\hat{\mathbf{P}}) Y_{l_j m_j}(\hat{\mathbf{P}}) d\Omega_{\mathbf{P}}. \quad (19)$$

It is convenient to separate the diagonal and off-diagonal parts in the above double sum, and to split the latter into sums involving single-centre and two-centre terms:

$$\rho(P) = \sum_i |c_i|^2 \rho_i(P) + \sum_{\substack{\mathbf{R}_i = \mathbf{R}_j \\ i, j > i}} \rho_{ij}^I(P) + \sum_{\substack{\mathbf{R}_i \neq \mathbf{R}_j \\ i, j \neq i}} \rho_{ij}^{II}(P). \quad (20)$$

In this equation, the second term on the right-hand side is a sum of the products of wavefunctions centred on the same atom. They satisfy the usual orthogonality relations and take the form

$$\rho_{ij}^I(P) = (c_i^* c_j + c_i c_j^*) \delta_{l_i l_j} \delta_{m_i m_j} \sqrt{\rho_i(P) \rho_j(P)}. \quad (21)$$

The third term on the right-hand-side of (20) is a sum over the product of wavefunctions centred on different atomic sites. Resolving the plane wave and expressing the integrals of three spherical harmonics in terms of  $3j$  symbols (see e.g. [48]), it can be written as

$$\begin{aligned} \rho_{ij}^{II}(P) &= \sqrt{4\pi} c_i^* c_j \sqrt{\rho_i(P) \rho_j(P)} (-1)^{m_i} \sum_{\lambda, \mu} (-1)^{(l_i - l_j + \lambda)/2} j_\lambda(P R_{ij}) Y_{\lambda \mu}^*(\hat{\mathbf{R}}_{ij}) \\ &\times \sqrt{[l_i][l_j][\lambda]} \begin{pmatrix} l_i & \lambda & l_j \\ -m_i & \mu & m_j \end{pmatrix} \begin{pmatrix} l_i & \lambda & l_j \\ 0 & 0 & 0 \end{pmatrix}, \end{aligned} \quad (22)$$

where  $\mathbf{R}_{ij} = \mathbf{R}_i - \mathbf{R}_j$  and we use the notation  $[l] \equiv (2l+1)$ .

$$G(P) \equiv \frac{\int \frac{d\Omega_{\mathbf{P}}}{4\pi} \left| \begin{array}{c} \varepsilon \\ \text{---} \end{array} \right. \times \text{---} \left. \begin{array}{c} \mathbf{P} \\ n \end{array} \right|^2}{\int \frac{d\Omega_{\mathbf{P}}}{4\pi} \left| \begin{array}{c} \varepsilon^{\text{PW}} \\ \text{---} \end{array} \right. \times \text{---} \left. \begin{array}{c} \mathbf{P} \\ n \end{array} \right|^2}; \quad G_0^{\text{HF}}(P) \equiv \frac{\int \frac{d\Omega_{\mathbf{P}}}{4\pi} \left| \begin{array}{c} \varepsilon^{\text{HF}} \\ \text{---} \end{array} \right. \times \text{---} \left. \begin{array}{c} \mathbf{P} \\ n \end{array} \right|^2}{\int \frac{d\Omega_{\mathbf{P}}}{4\pi} \left| \begin{array}{c} \varepsilon^{\text{PW}} \\ \text{---} \end{array} \right. \times \text{---} \left. \begin{array}{c} \mathbf{P} \\ n \end{array} \right|^2}$$

**Figure 4.** Atomic correction factors: (a) the ‘exact’ atomic correction factor for atomic orbital  $n$ , defined as  $G(P) \equiv \rho_n^a(P)/\rho_n(P)$ , where  $\rho_n^a$  is calculated using the positron Dyson orbital and the full vertex (see figure 1); (b) the simpler HF correction factor defined as  $G_0^{\text{HF}}(P) \equiv \rho_n^{a,\text{HF}}(P)/\rho_n(P)$ , where  $\rho_n^{a,\text{HF}}(P)$  is calculated with a HF positron wavefunction and the zeroth-order annihilation vertex.

To summarize, in the LCAO approach the *molecular* orbital momentum density is determined by the products of the relevant *atomic* momentum densities,

$$\rho(P) = \sum_{i,j \geq i} C_{ij}(c_i, P, \mathbf{R}_{ij}) \sqrt{\rho_i(P)\rho_j(P)}, \quad (23)$$

where  $C_{ij}$  are the prefactors given in equations (20)–(22). This quantity represents the annihilation momentum density for the corresponding molecular orbital in the low-energy plane-wave-positron approximation. A more accurate molecular annihilation spectrum will be obtained by replacing the atomic electron momentum densities in (23) by the corresponding annihilation momentum densities.

#### 4.2. Atomic correction factors

To include the effects of the positron–atom interactions in the molecular annihilation momentum density, the plane-wave *atomic* electron momentum densities  $\rho_i(P)$  that appear in (23) are multiplied by the *atomic correction factor*, defined as

$$G_i(P) \equiv \frac{\rho_i^a(P)}{\rho_i(P)}, \quad (24)$$

i.e. as the ratio of the true annihilation momentum density of the atomic orbital  $i$  to its plane-wave independent-particle approximation.

For atomic hydrogen, the correction factors can be calculated accurately from many-body theory (see figure 4(a) for a diagrammatic definition). They therefore include the effect of electron–positron and positron–atom correlations, in addition to that of the nuclear repulsion. A simpler correction factor that can be used for any atom and still include the effect of the atomic potential and nuclear repulsion can be obtained using a HF positron function with the zeroth-order (independent-particle) annihilation vertex (see figure 4(b)). Note that the effect of the short-range electron–positron correlations are not included in this correction factor.

We will apply this procedure to calculate the  $\gamma$ -spectra of  $\text{H}_2$ ,  $\text{CH}_4$  and  $\text{CF}_4$ . Figures 5 and 6 show the atomic correction factors for hydrogen, carbon and fluorine, calculated for the  $s$ -wave positron wavefunction which dominates at the low (room-temperature) momentum  $k = 0.04 \text{ au}$ .

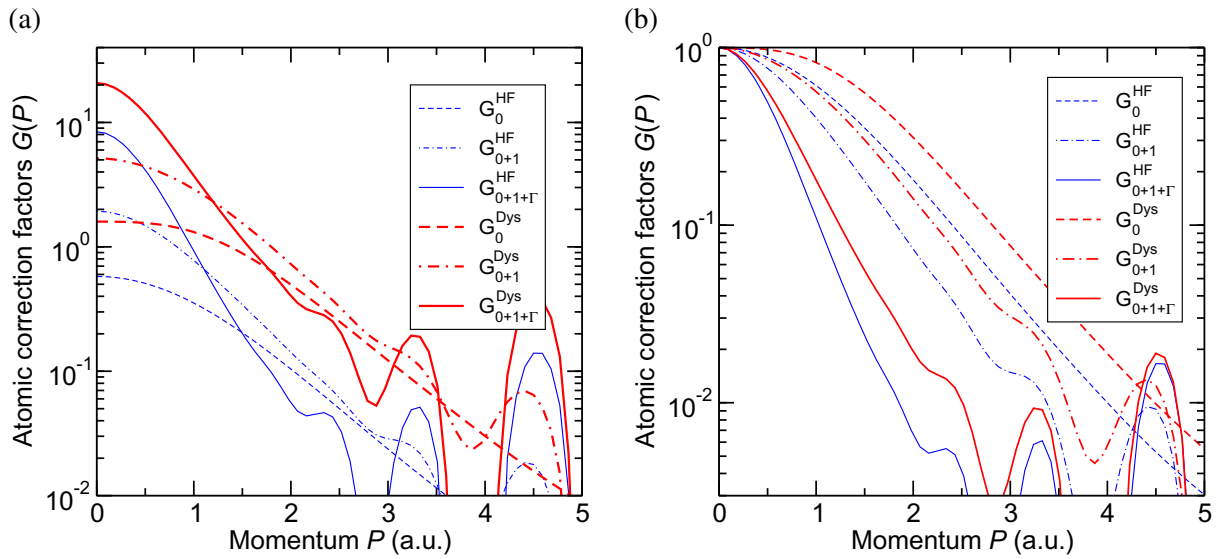


**Figure 5.** Momentum-dependent atomic correction factors for hydrogen: (a) absolute values; (b) normalized to unity at  $P = 0$ . The various approximations correspond to the static-field HF (thin blue lines) and Dyson (thick red lines) positron orbitals and different approximations to the annihilation vertex (see figure 1): 0th-order (---), 0th+1st order (—·—), and 0th+1st+ $\Gamma$  (—). The oscillations in the tails are artefacts arising from computational ‘noise’ in the many-body theory calculations.

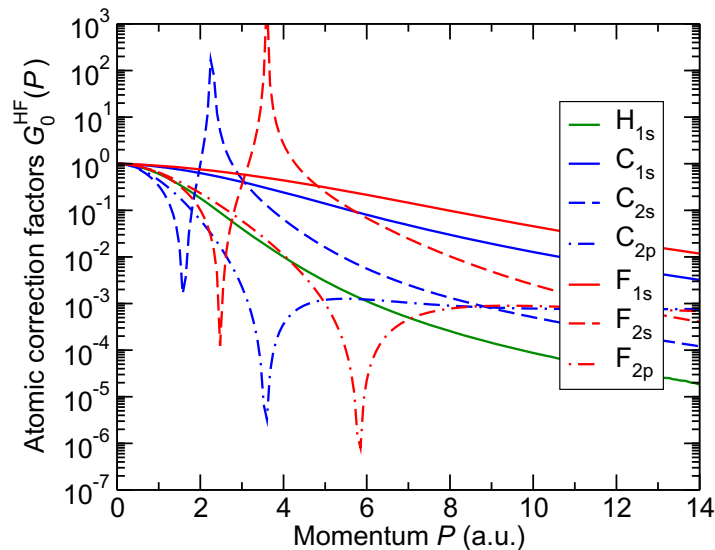


**Figure 6.** Momentum-dependent atomic correction factors for the ground state orbitals of hydrogen, carbon and fluorine calculated using the HF positron wavefunction with the zeroth-order annihilation vertex. All correction factors are normalised to unity at  $P = 0$ .

Figure 5 shows the correction factor for hydrogen calculated using different approximations to the annihilation vertex and positron wavefunction. Figure 5(a) shows the absolute values of the correction factors. The factors calculated using Dyson positron quasiparticle wavefunction are larger than those calculated with the HF orbital, due to the inclusion of the attractive self-energy in the former. For a given positron wavefunction, the inclusion of the corrections to the annihilation vertex dramatically increases the correction factors at small momenta, owing to the increased attraction between the electron and positron. From equation (11) it is clear that using larger magnitude correction factors will lead to corresponding increases in the annihilation rate, as documented in table 2.

The effect that these factors have on the *shape* of  $\gamma$ -spectra is most easily inferred from figure 5(b), in which the factors are normalized to unity at  $P = 0$ . The effect of the nuclear repulsion is most easily seen through the zeroth-order factor  $G_0^{\text{HF}}$ . The shape of this factor is mainly governed by the nuclear repulsion, the effect of which is evidently to suppress the high-momentum regions of the momentum density. Further suppression results from inclusion of the additional correlations. One can also see that for a given approximation to the positron wavefunction, adding the first-order and higher-order ( $\Gamma$ -block) correlation corrections to the vertex increases the degree of suppression of high momentum components to the annihilation momentum density. Physically, this is explained by noting that the corrections to the vertex involve positron annihilation with spatially diffuse virtual electrons. On the other hand, using the correlated positron Dyson orbital instead of the HF (i.e. static field) positron wavefunction increases the high-momentum component for a given approximation for the vertex. Again this is what one should expect physically, since the inclusion of the attractive correlational potential accelerates the positron towards the atom and increases the momentum of the annihilating electron–positron pair. Regarding the  $\gamma$ -spectrum shape therefore, there is some compensation between including the correlation corrections to the vertex and increasing the accuracy of the positron wavefunction. However, the dominant effect of  $G(P)$  is always the suppression of high momenta.

For the carbon and fluorine atoms, we have only the zeroth-order HF correction factors at our disposal<sup>11</sup> and these are shown for the ground states orbitals in figure 6. Note that the correction factors for the 2s orbitals show singularities arising from the nodes in the HF wavefunctions (which result in the zeros of the corresponding electron momentum densities  $\rho_{2s}(P)$ ). Nevertheless, the suppression of high momentum contributions to the spectra is clear. Moreover, when evaluating the  $\gamma$ -spectra in the LCAO approach we circumvent the problem of the singularities in the correction factors by simply replacing the atomic electron momentum densities with the annihilation momentum densities, i.e. we calculate  $\rho_i^a(P)$  directly rather than  $\rho_i(P)G_i(P)$ . For carbon and fluorine, the positrons predominantly annihilate on the valence electrons. The magnitude of the correction factor for the valence electrons is therefore substantially greater than for the core electrons.

Finally, although for hydrogen the correction factors are sensitive to the positron–atom and positron–electron correlations, for heavier atoms most of the suppression at high momenta is due to the effect of the nuclear repulsion. Hence, for such atoms the HF correction factor will describe the true suppression more accurately than it does for hydrogen. This point will be discussed further in section 5.

<sup>11</sup> The many-body theory cannot be applied directly to open-shell atoms, but the static-field effect is the dominant feature for higher- $Z$  atoms and core orbitals.

## 5. Gamma spectra with atomic correction factors

### 5.1. Molecular hydrogen

**5.1.1. Gamma spectrum of  $H_2$ .** In the LCAO approximation, the ground state molecular orbital  $\psi_{\sigma_g}(\mathbf{r})$  can be written a linear combination of two hydrogenic 1s orbitals, each centred on one of the protons,

$$\psi_{\sigma_g}(\mathbf{r}) = \frac{1}{\sqrt{2(1+S)}} [\psi_{1s}(\mathbf{r} - \mathbf{R}_1) + \psi_{1s}(\mathbf{r} - \mathbf{R}_2)], \quad (25)$$

where  $\psi_{1s}(\mathbf{r}) = (\pi\alpha^3)^{-1/2}e^{-\alpha r}$  and  $S$  is the overlap integral  $\int \psi_{1s}(\mathbf{r} - \mathbf{R}_1)\psi_{1s}(\mathbf{r} - \mathbf{R}_2) d^3r$ . It can be calculated analytically using prolate spheroidal coordinates as  $S = e^{-\alpha R} [1 + \alpha R + \frac{1}{3}(\alpha R)^2]$ , where  $R$  is the internuclear distance [49]. A variational calculation gives  $\alpha \approx 1.19$  for  $R = 1.38$  au, and therefore,  $S \approx 0.69$  [50].

Substituting (25) into (20) gives the molecular orbital momentum density

$$\rho_{\sigma_g}(P) = \frac{1}{1+S} \rho_{1s}(P) [1 + j_0(PR)], \quad (26)$$

where  $\rho_{1s}(P)$  is the momentum density of the hydrogenic 1s orbital,

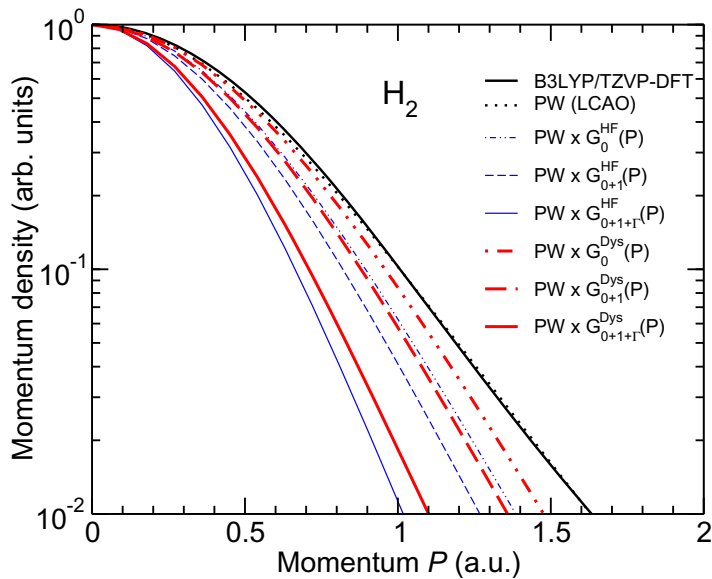
$$\rho_{1s}(P) = \frac{8\alpha^5}{\pi^2(\alpha^2 + P^2)^4}. \quad (27)$$

Figure 7 shows that the LCAO molecular orbital density given by (26) is very close to that from B3LYP/TZVP density functional theory calculation.

Figure 7 also shows the hydrogen molecule annihilation momentum densities obtained from (26) by scaling the atomic momentum density with the correction factors  $G(P)$  obtained from many-body-theory calculations using various approximations to the annihilation vertex and positron wavefunction (cf figure 5), i.e. by substitution  $\rho_{1s}(P) \rightarrow G(P)\rho_{1s}(P)$ . To emphasize the effect of the correction factors on the annihilation momentum density, all densities are normalized to unity at  $P = 0$ . As expected, the use of correction factors leads to significant narrowing of the momentum distribution.

The corresponding annihilation  $\gamma$ -spectra are shown in figure 8, where they are compared with the experimental result of Iwata *et al* [3]. The FWHM values of the  $\gamma$ -spectra are given in table 2. The spectra obtained from the B3LYP/TZVP and LCAO electron momentum densities are practically indistinguishable, and we show only the latter in the figure. This ‘low-energy plane-wave positron’ calculation gives the FWHM value about 35% greater than experiment. As discussed above, this overestimation of the high-momentum contribution is largely due to the neglect of the positron–nuclear repulsion. Introducing the effects of the nuclear repulsion through the zeroth-order vertex HF correction factor  $G_0^{\text{HF}}$ , narrows the spectrum, but it remains  $\approx 18\%$  broader than experiment. Using the most accurate, ‘exact’ atomic adjustment factor  $G_{0+1+\Gamma}^{\text{Dys}}(P)$  gives a spectrum that is in very good agreement with measured one at energy shifts below 2 keV. At larger Doppler shifts there is a noticeable discrepancy between the ‘exact’ adjustment factor result and experiment. However, in this energy range our approach may be deficient, and the shape of the experimental spectrum may be affected by the limitation of the two-Gaussian fit.

The final theoretical FWHM is in good agreement (within 6%) with the measured value. One can see that for  $H_2$ , the inclusion of the nuclear repulsion provides only 50% of the



**Figure 7.** Hydrogen molecule electron momentum densities calculated using the B3LYP DFT (black solid curve) and LCAO, (26) (· · · · ·), and annihilation momentum densities obtained from (26) by multiplying the ‘plane-wave’ (PW) atomic density  $\rho_{1s}(P)$  by the correction factors  $G(P)$  obtained from many-body-theory calculations using different approximations to the positron wavefunction, i.e. HF (thin blue lines) and Dyson (thick red lines), and the annihilation vertex (see figure 1): 0th (— · —), 0th + 1st (---) and 0th + 1st +  $\Gamma$  (—). All densities are normalized to unity at  $P = 0$ .

narrowing required to bring the plane-wave calculation into agreement with experiment, with the remaining 50% being due to the electron–positron correlations. However, as the nuclear potential becomes stronger in molecules containing heavier atoms, the effect of the potential on the linewidth is expected to become the principal cause of the narrowing, overriding the effect of the correlations.

Using  $H_2$  as an example, we can examine a simpler method in which the correction factor is applied directly to the Doppler-shift spectrum rather than to the two- $\gamma$  momentum density. The method is suggested by an observation that the momentum densities and the  $\gamma$ -spectra in figures 7 and 8 are approximately Gaussian (i.e. parabolic in the semilogarithmic plots). If one assumes that both the electron momentum and the true annihilation momentum *atomic* densities are Gaussians, then the atomic correction factor  $G(P)$ , (24), will also be a Gaussian. It is easy to see from equations (5) and (10) that in this case the corresponding annihilation spectra are also Gaussian. Their widths are proportional to those of the momentum densities (scaled by  $c/2$ ). Denoting the FWHM values of the true annihilation spectrum and that found using the electron momentum density by  $\sigma_a$  and  $\sigma_m$ , we can introduce the atomic  $\gamma$ -spectrum correction factor  $G_\gamma(\epsilon) \equiv w(\epsilon)/w_m(\epsilon)$ , which will also be a Gaussian, of width  $\sigma_G = (\sigma_a^{-2} - \sigma_m^{-2})^{-1/2}$ .

This means that if the  $\gamma$ -spectrum of *molecular* hydrogen calculated using the electron momentum density (i.e. plane-wave positron) is close to a Gaussian, of width  $\sigma_m^{H_2}$ , then one can approximate the true annihilation  $\gamma$ -spectrum of  $H_2$  by  $w^{H_2}(\epsilon) \approx G_\gamma(\epsilon)w_m^{H_2}(\epsilon)$ . The latter will

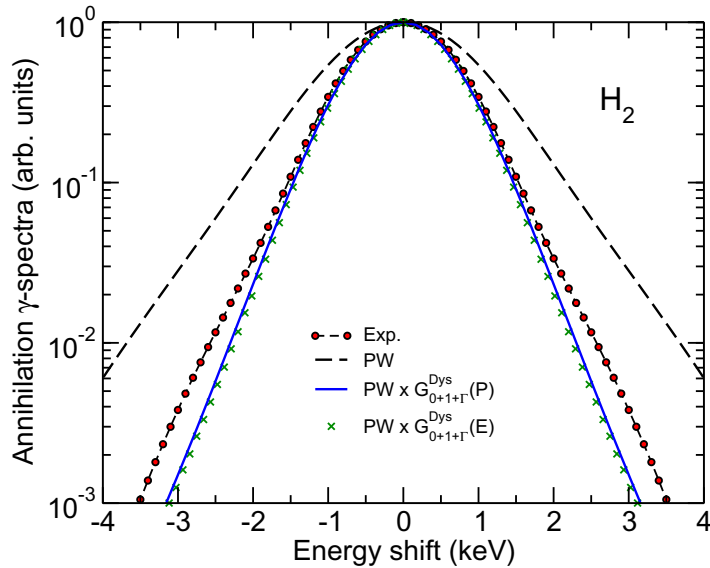


**Figure 8.** Annihilation  $\gamma$ -spectra of  $\text{H}_2$  calculated using LCAO in the plane-wave-positron approximation, i.e. using the density from (26) (long-dashed line), and incorporating the ‘exact’ momentum-dependent atomic correction factor  $G_{0+1+\Gamma}^{\text{Dys}}(P)$  (solid line) and the energy-shift-dependent correction factor  $G_\gamma(\epsilon)$  (crosses, see text); solid circles show the measured spectrum, as represented by the two-Gaussian fit [3]. All spectra are normalized to unity at  $\epsilon = 0$ .

also be a Gaussian with the width

$$\sigma_a^{\text{H}_2} = \left[ \frac{1}{(\sigma_m^{\text{H}_2})^2} + \frac{1}{\sigma_G^2} \right]^{-1/2} = \frac{\sigma_m^{\text{H}_2}}{\sqrt{1 + (\sigma_m^{\text{H}_2}/\sigma_G)^2}}. \quad (28)$$

Figure 8 shows that adjusting the the spectrum by the Doppler-shift-dependent correction factor  $G_\gamma(\epsilon)$  for  $\text{H}_2$  produces a spectrum in good agreement with the result obtained using  $G(P)$  and with experiment.

Estimating the width of  $G_\gamma(\epsilon)$  from the best calculation shown in figure 6 ( $G_{0+1+\Gamma}^{\text{Dys}}$ ) gives  $\sigma_G = 2.10 \text{ keV}$ . Using this value together with the plane-wave-positron width  $\sigma_m^{\text{H}_2} = 2.14 \text{ keV}$  (table 2) in (28) gives the annihilation spectrum width  $\sigma_a^{\text{H}_2} \approx 1.50 \text{ keV}$ , in agreement with the best calculated value in table 2.

This example shows that  $\sigma_G \approx \sigma_m$ , i.e. that the width of the positron atomic correction factor is close to the that of the electron momentum distribution. In this case the expression under the square root in (28) is close to 2, giving  $\sigma_a \approx \sigma_m/1.4$ . It appears that this relation is quite general, as shown by the FWHM values for other molecules and atoms in table 1 and figure 3. This suggests that to obtain a closer description of experiment, the spectra calculated neglecting the positron can be modified by simply scaling the energy shift by a factor 1.4. The corresponding spectra are shown in figure 2 by dotted lines. The agreement with experiment is excellent for hydrogen and good for alkanes (except in the wings), with larger discrepancies for molecules containing fluorine atoms.

**Table 2.** FWHM of the annihilation  $\gamma$ -spectra and annihilation rate parameter  $Z_{\text{eff}}$  for  $H_2$  calculated in the plane-wave positron approximation (B3LYP/TZVP DFT and LCAO) and using the atomic correction factors in different approximations, and results of other theoretical calculations and experiments.

Method	FWHM	
	(keV)	$Z_{\text{eff}}$
B3LYP/TZ-DFT (plane-wave) <sup>a</sup>	2.14	2.00
LCAO (plane-wave) <sup>a</sup>	2.14	2.00
$\text{LCAO} \times G_0^{\text{HF}}(P)^a$	1.88	0.78
$\text{LCAO} \times G_{0+1}^{\text{HF}}(P)^a$	1.73	1.98
$\text{LCAO} \times G_{0+1+\Gamma}^{\text{HF}}(P)^a$	1.40	4.59
$\text{LCAO} \times G_0^{\text{Dys}}(P)^a$	2.01	2.62
$\text{LCAO} \times G_{0+1}^{\text{Dys}}(P)^a$	1.85	6.54
$\text{LCAO} \times G_{0+1+\Gamma}^{\text{Dys}}(P)^a$	1.50	13.9
Kohn variational <sup>b</sup>	–	10.3
Kohn variational <sup>c</sup>	–	9.8
Kohn variational <sup>d</sup>	–	12.6
Stochastic variational <sup>e</sup>	–	15.7
Molecular $R$ -matrix <sup>f</sup>	–	10.4
Expt. <sup>g</sup>	1.59	–
Expt. <sup>h</sup>	–	14.7
Expt. <sup>i</sup>	–	16.0
Expt. <sup>j</sup>	–	14.6

<sup>a</sup> This study,  $R = 1.4$  au,  $k = 0.04$  au.

<sup>b</sup> ‘Method of models’ calculation from [51].

<sup>c</sup> Calculation for  $R = 1.4$  au,  $k = 0.04$  au [52].

<sup>d</sup> ‘Method of models’ calculation from [53].

<sup>e</sup> Confined variational method calculation [54].

<sup>f</sup> Molecular  $R$ -matrix with pseudo-states [55].

<sup>g</sup> Experiment, room-temperature positrons [3].

<sup>h</sup> Experiment, room-temperature positrons [56].

<sup>i</sup> Experiment, room-temperature positrons [57].

<sup>j</sup> Experiment, room-temperature positrons [58].

**5.1.2.  $Z_{\text{eff}}$  of  $H_2$ .** The correction factor approach also provides a means of estimating the normalized annihilation rate parameter  $Z_{\text{eff}}$  for positrons on  $H_2$ . Its accurate theoretical calculation has proved to be a difficult problem to which considerable attention has been paid. Extensive calculations have been performed by Armour *et al* [51–53], who have applied various versions of the Kohn variational method. However, their best theoretical results still underestimate commonly accepted measured value of 14.6 [58]. Only recently has this problem been effectively solved, with Zhang *et al* [54] performing a stochastic variational method calculation which provided an accurate total wavefunction of this two-electron–one-positron system and yielded a low-energy (thermalized)  $Z_{\text{eff}}$  of 15.7.

In this work we calculate the  $Z_{\text{eff}}$  from the  $\gamma$ -spectrum using (11). The results of the B3LYP/TZVP DFT and LCAO calculations using the atomic correction factors are given in table 2. As one should expect, the plane-wave positron approximation (both B3LYP/TZVP and LCAO) gives  $Z_{\text{eff}} = 2$ , i.e. the number of electrons. The effect of the repulsive atomic field, implicit in  $G_0^{\text{HF}}$ , reduces the magnitude of  $Z_{\text{eff}}$  by more than a factor of two relative to the plane-wave calculation, owing to the reduced overlap between the electrons and the incident positron. However, the successive inclusion of higher-order correlation effects through the correction factors produces a marked increase in the calculated  $Z_{\text{eff}}$ , with the full many-body theory (Dyson positron orbital, exact vertex) giving  $Z_{\text{eff}} = 13.9$ , which is within 5% of the measured value. This level of agreement is partly fortuitous, but it is still remarkable that the calculation which uses atomic correction factors gives a molecular  $Z_{\text{eff}}$  value in such close agreement with experiment. The fact that it does give some *a posteriori* justification for the LCAO correction factor approach and its ability to take appropriate account of the positron-molecule and positron-electron correlations in H<sub>2</sub>.

### 5.2. Gamma spectrum of methane

Methane, CH<sub>4</sub>, has a tetrahedral structure with a point group  $T_d$ . The four hydrogenic 1s orbitals span the reducible representation  $\Gamma_{\sigma}^{\text{red}} = A_1 \oplus T_2$ , where  $A_1$  is the fully symmetric one-dimensional representation and  $T_2$  is a degenerate three-dimensional representation. Denoting the carbon ground state orbitals by  $\psi_{nl}$  and the four atomic hydrogen ground-state orbitals by  $\sigma_i$ , the ground state molecular LCAO of methane are (see e.g. [59])

$$\psi_{1a_1}(\mathbf{r}) = \alpha_1 \psi_{1s} + \beta_1 \psi_{2s} + \gamma_1 \sigma^{A_1}, \quad (29)$$

$$\psi_{2a_1}(\mathbf{r}) = \alpha_2 \psi_{1s} + \beta_2 \psi_{2s} + \gamma_2 \sigma^{A_1}, \quad (30)$$

$$\psi_{1t_{2x,y,z}}(\mathbf{r}) = \delta \psi_{2p_{x,y,z}} + \gamma_3 \sigma_x^{T_2}, \quad (31)$$

where  $\alpha$ ,  $\beta$ ,  $\gamma$  and  $\delta$  are the expansion coefficients and the symmetry adapted linear combinations (SALC) of pendant atoms are given by

$$\sigma^{A_1}(\mathbf{r}) = \sigma_1 + \sigma_2 + \sigma_3 + \sigma_4,$$

$$\sigma_x^{T_2}(\mathbf{r}) = \sigma_1 - \sigma_2 - \sigma_3 + \sigma_4,$$

$$\sigma_y^{T_2}(\mathbf{r}) = \sigma_1 + \sigma_2 - \sigma_3 - \sigma_4,$$

$$\sigma_z^{T_2}(\mathbf{r}) = \sigma_1 - \sigma_2 + \sigma_3 - \sigma_4.$$

The total electron momentum density for methane is given by the sum of the respective individual molecular orbital densities,

$$\rho(P) = 2\rho_{1a_1}(P) + 2\rho_{2a_1}(P) + 6\rho_{1t_2}(P), \quad (32)$$

obtained from equations (29)–(31) and (20) in terms of the atomic orbital momentum densities, as

$$\begin{aligned} \rho_{na_1}(P) &= \alpha_n^2 \rho_{1s}^C(P) + \beta_n^2 \rho_{2s}^C(P) + 2\alpha_n \beta_n \sqrt{\rho_{1s}^C(P) \rho_{2s}^C(P)} + 4\gamma_n^2 \rho_{1s}^H(P) [1 + 3 j_0(P R_{\text{HH}})] \\ &\quad + 8 j_0(P R_{\text{CH}}) \gamma_n \sqrt{\rho_{1s}^H(P)} \left[ \alpha_n \sqrt{\rho_{1s}^C(P)} + \beta_n \sqrt{\rho_{2s}^C(P)} \right], \end{aligned} \quad (33)$$

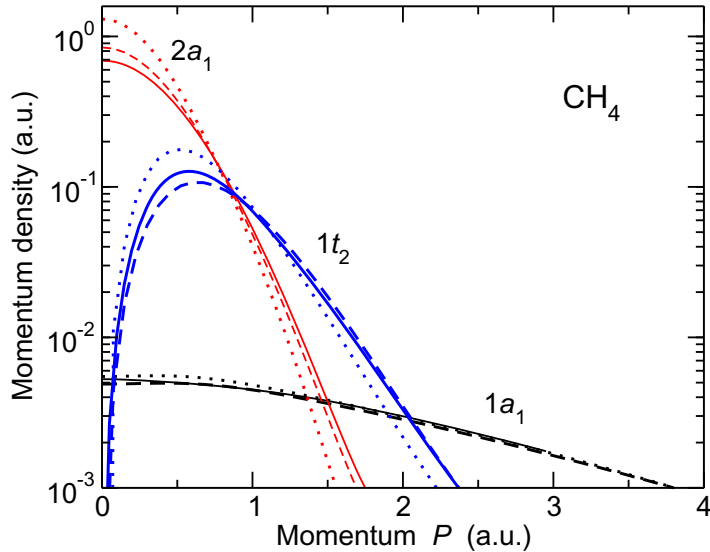


**Figure 9.** Electron momentum densities (i.e. plane-wave positron annihilation momentum densities) for the molecular orbitals of methane: (solid lines) B3LYP/TZVP; (dashed lines) Slater-type orbitals; (dotted lines) HF.

$$\rho_{1t_2}(P) = \delta^2 \rho_{2p}^C(P) + 4\gamma_3^2 \rho_{1s}^H(P) [1 - j_0(PR_{HH})] + 8\gamma_3 \delta j_1(PR_{CH}) \sqrt{\rho_{2p}^C(P) \rho_{1s}^H(P)}, \quad (34)$$

where  $R_{CH}$  and  $R_{HH}$  are the C–H and H–H bond lengths, respectively.

We construct the molecular orbitals of equations (29)–(31) in two ways. In the first case, we use Slater-type atomic orbitals (LCAO-STO) optimized for the molecular environment [60]. In the second case, we use HF atomic orbitals (LCAO-HF). In both cases the LCAO expansion coefficients are taken to be those of [60], with a C–H distance of  $R_{CH} = 2.05$  au.

Figure 9 shows the electron momentum densities calculated using the DFT based B3LYP/TZVP model, and the LCAO result from (32) using the Slater-type and HF orbitals. For a given molecular orbital, the results of all three calculations are similar. However, in general the LCAO-STO calculation is in better agreement with the B3LYP/TZVP calculation than the LCAO-HF one, owing to the fact that the HF orbitals used are purely atomic in nature, i.e. they are in no way adjusted to account for the molecular environment.<sup>12</sup> Note that the momentum density of the  $1a_1$  orbital (predominantly carbon 1s in nature) is much broader than those of the valence  $2a_1$  and  $1t_2$  orbitals due to the fact that the core electrons have larger characteristic momenta.

To take into account the effect of the positron–atom interactions on the annihilation momentum density and  $\gamma$ -spectrum, we replace the atomic electron momentum densities in equations (33) and (34) by the corresponding annihilation momentum densities calculated using the HF positron wavefunction. These are then used in equation (32) and the annihilation spectrum is found from equation (5). This procedure is equivalent to the use of atomic correction factors  $G_0^{HF}(P)$ , which is expected to narrow the spectrum (see figure 6).

<sup>12</sup> This is in contrast with the treatment of  $H_2$  in section 5.1, where we used hydrogenic orbitals with  $\alpha = 1.19$  from a variational calculation, rather than those of the H atom ( $\alpha = 1$ ).

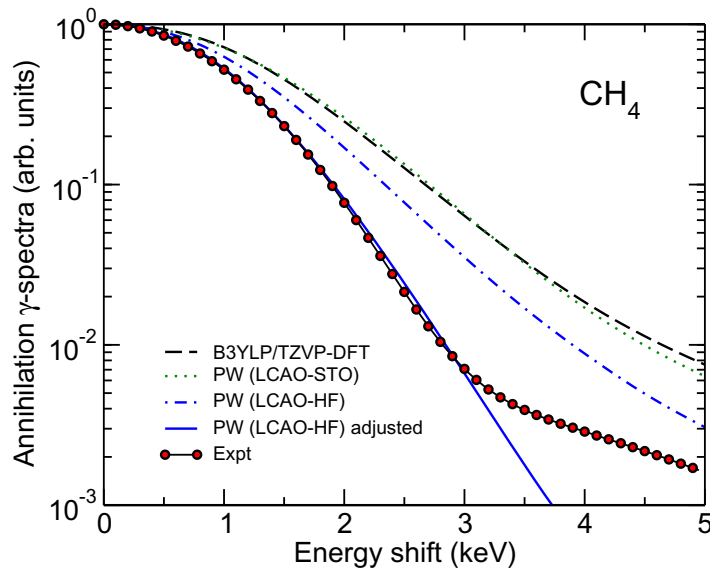


**Figure 10.** Annihilation  $\gamma$ -spectra of  $\text{CH}_4$ : (dashed line) B3LYP calculation; (dotted line) LCAO-STO; (dot-dashed line) LCAO-HF (all correspond to the low-energy plane-wave positron); (thick solid) LCAO-HF using the atomic annihilation momentum densities; (circles) experiment, two-Gaussian fit [3]. All spectra are normalized to unity at  $\epsilon = 0$ .

**Table 3.** FWHM of the  $\gamma$ -spectra for  $\text{CH}_4$  (in keV).

Orbital	B3LYP	LCAO			Exp.
		STO	HF	HFa	
$2a_1$	1.96	1.85	1.64	1.45	–
$1t_2$	3.31	3.52	2.98	2.55	–
Total (valence)	2.81	2.85	2.43	2.09	–
Total (all)	2.97	2.97	2.52	2.09	2.06

<sup>a</sup> Corrected by using the atomic annihilation momentum densities.

Figure 10 shows the annihilation  $\gamma$ -spectra of  $\text{CH}_4$ , calculated using the B3LYP/TZVP and LCAO (both STO and HF), and the LCAO-HF results corrected for the positron–atom interactions, as well as the measured spectrum. The B3LYP/TZVP spectrum is significantly broader than the measured one, as seen earlier in figure 2. The fact that the LCAO-STO result is in very good agreement with the B3LYP/TZVP result confirms the applicability of the LCAO approach. The LCAO-HF spectrum calculated in the same low-energy plane-wave positron approximation (i.e. neglecting the positron wavefunction) is narrower than B3LYP/TZVP, but still much broader than experiment. The overestimation of the width must therefore originate from the neglect of the positron wavefunction. Note that the plane-wave calculation overestimates the spectral FWHM significantly, even when the  $1a_1$  core orbital is neglected (see table 3).

Correcting the LCAO-HF spectrum by using atomic annihilation momentum densities in equations (32)–(34) produces a  $\gamma$ -spectrum which is very close to experiment for Doppler shifts smaller than 3 keV (solid line in figure 10). The excellent agreement with experiment is somewhat fortuitous because the starting point for the adjustment, i.e. the plane-wave LCAO-HF calculation, does not perfectly agree with the accurate B3LYP/TZVP molecular calculation. However, the need for and effect of the correction is clear. As can be seen in table 3, a considerable narrowing is observed with the FWHM reduced from 2.52 to 2.09 keV, compared with the measured value of 2.06 keV. Thus most of the required narrowing to obtain agreement with experiment has been accounted for through the effective inclusion of the nuclear repulsion with all of the atoms. In the case of H<sub>2</sub> we saw that electron-positron annihilation vertex corrections further narrow the annihilation spectrum (see figure 5). Therefore, it is expected that if one combined more accurate atomic correction factors with the broader LCAO-STO (or B3LYP/TZVP) electron momentum density (see figure 10), the resulting annihilation spectrum would provide a good description of the experimental data.

Finally, note that a broad core contribution can be seen clearly in the experimental spectrum for Doppler shifts  $> 3$  keV. To reproduce this feature, the theory would need to be able to calculate accurately the size of the core contribution relative to that of the valence molecular orbitals [8].

### 5.3. Gamma spectrum of tetrafluoromethane

Like methane, tetrafluoromethane (CF<sub>4</sub>) belongs to the point group  $T_d$ . Similar to the hydrogens in CH<sub>4</sub>, the groups of fluorine 1s, 2s and 2p<sub>*z*</sub> orbitals (with the *z* axis directed locally towards the carbon atom) span the reducible representation  $\Gamma_{\sigma}^{\text{red}} = A_1 \oplus T_2$ . In contrast to CH<sub>4</sub>, for CF<sub>4</sub> one has the additional complication of  $\pi$  bonding, with the complete set of the eight fluorine 2p<sub>*x,y*</sub> orbitals forming a basis for a reducible representation  $\Gamma_{\pi}^{\text{red}} = E \oplus T_1 \oplus T_2$  (see e.g. [50, 59]). Accordingly, the B3LYP/TZVP calculation for CF<sub>4</sub> gives the following electronic orbital structure: core +1a<sub>1</sub><sup>2</sup> 1t<sub>2</sub><sup>6</sup> 2a<sub>1</sub><sup>2</sup> 2t<sub>2</sub><sup>6</sup> e<sup>4</sup> 3t<sub>2</sub><sup>6</sup> t<sub>1</sub><sup>6</sup>, where the core consists of a triply degenerate  $T_2$  symmetry orbital and a fully symmetric orbital that are predominantly F 1s in nature, and another fully symmetric orbital which is predominantly C 1s in nature. Owing to the repulsion from the nuclei, the positron will have difficulty reaching and subsequently annihilating on these core orbitals, and the effect of the correction factors will be to greatly suppress the magnitude of the contribution of these core orbitals in comparison with the valence orbitals.

To employ the momentum-dependent correction factors, note that the *e* and *t*<sub>1</sub> molecular orbitals are nonbonding, and are composed entirely of F 2p orbitals. Their respective electron-momentum densities can therefore simply be multiplied by  $G_{\text{F2p}}(P)$  when calculating the corrected annihilation spectra. To apply the correction to the remaining molecular orbitals, however, we must construct the LCAO molecular orbitals and replace the electron momentum densities with the annihilation momentum densities calculated, in this case, in the HF zeroth-order vertex approximation, as was done for CH<sub>4</sub>. The molecular orbitals are

$$\begin{aligned}\psi_{a_1} &= \alpha_1 \psi_{C1s} + \beta_1 \psi_{C2s} + \gamma_1 \sigma_{\text{F1s}}^{A_1} + \delta_1 \sigma_{\text{F2s}}^{A_1} + \eta_1 \sigma_{\text{F2p}_z}^{A_1}, \\ \psi_{t_{2x,y,z}} &= \alpha_2 \psi_{C2p} + \beta_2 \sigma_{\text{F2p}_{x,y,z}}^{T_2} + \gamma_2 \sigma_{\text{F2p}_{x,y,z}}^{T_2} + \delta_2 \pi_{\text{F2p}_{x,y,z}}^{T_2},\end{aligned}$$

where  $\alpha$ ,  $\beta$ ,  $\gamma$ ,  $\delta$  and  $\eta$  are the expansion coefficients, and the  $\sigma$  and  $\pi$  SALC orbitals are given in [61].

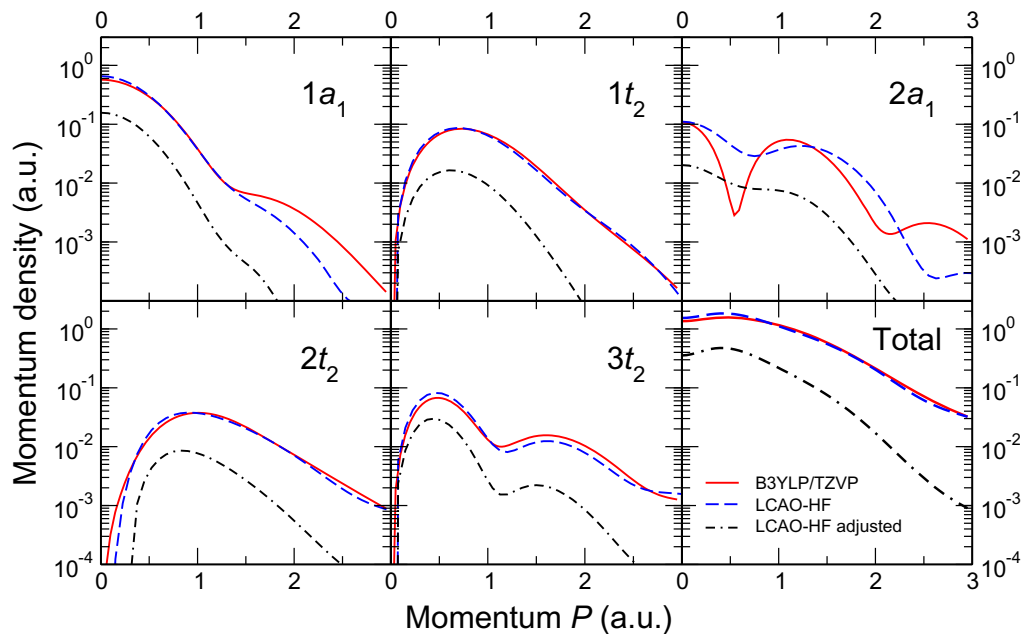


**Figure 11.** Electron momentum density of the valence orbitals of  $\text{CF}_4$  calculated using the B3LYP (solid lines) and the LCAO-HF approach (dashed lines). Dot-dashed lines show the annihilation momentum densities obtained in the LCAO-HF approach using atomic orbital correction factors.

Figure 11 shows the momentum densities for the valence molecular orbitals calculated in the LCAO approach from (20) using the HF atomic orbitals. We determined the coefficients in the LCAO expansions by fitting the LCAO-HF momentum densities to the accurate B3LYP results (see figure 11), using the coefficients from [61] as the starting approximation. This approach yields the LCAO-HF electron momentum densities in good agreement with the B3LYP results, especially for the  $t_2$  orbitals which contain most of the electrons. The total valence electron momentum density obtained in the LCAO-HF approach is very close to that of the B3LYP calculation. Also shown in figure 11 are the annihilation momentum densities obtained in the LCAO-HF approach using atomic annihilation momentum densities from the zeroth-order HF calculation (i.e. including the  $G_0^{\text{HF}}(P)$  factors for the atomic orbitals involved). As expected, the correction factors reduce the magnitudes of the momentum densities (because of the positron repulsion from the nuclei) and, in particular, suppress the contribution of high momenta.

Figure 12 shows the calculated annihilation  $\gamma$ -spectra along with the measured spectrum. The corresponding FWHM values are given in table 4. The spectra from the B3LYP and LCAO-HF calculations, which neglect the positron-molecule interaction, are in good agreement with each other, but are significantly broader than the experiment. On the other hand, the LCAO-HF calculation that incorporates the atomic correction factors gives results much closer to the measured spectrum. For  $\text{CF}_4$ , the dominant contribution to the annihilation momentum density comes from the twenty fluorine 2p electrons. Therefore, in addition, the figure shows the result of a simplified LCAO-HF calculation in which we use the correction factor of the fluorine 2p atomic orbital for *all* molecular orbitals. The results of both adjustment methods are very similar.

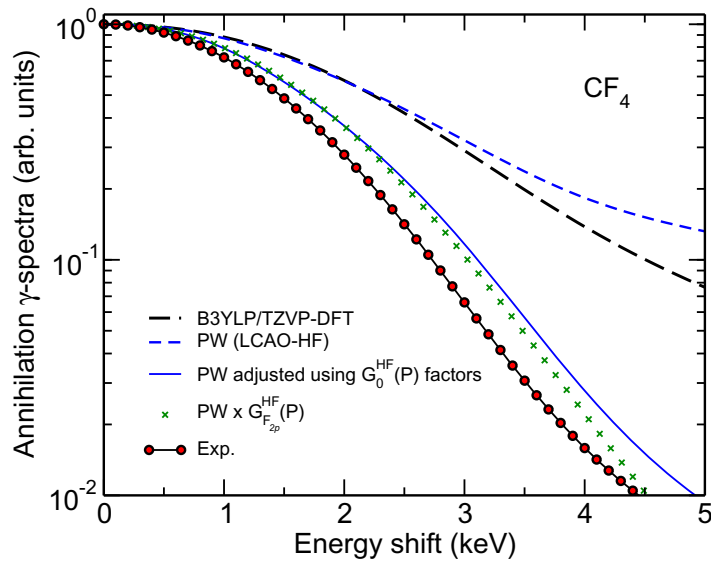


**Figure 12.** Annihilation  $\gamma$ -spectra of  $\text{CF}_4$ : (long-dashed line) B3LYP calculation; (short-dashed line) LCAO-HF (both correspond to the low-energy plane-wave positron approximation); (solid line) LCAO-HF with atomic correction factors; (crosses) LCAO-HF with the fluorine 2p-orbital correction factor; (circles) experiment, two-Gaussian fit [3]. The spectra were calculated from the total densities shown in figure 11 with power-type momentum density tails, and normalized to unity at  $\epsilon = 0$ .

**Table 4.** FWHM of the  $\gamma$ -spectra of  $\text{CF}_4$  (in keV).

B3LYP	LCAO			
	HF	HF <sup>a</sup>	HF <sup>b</sup>	Exp.
4.48	4.52	3.32	3.17	2.92

<sup>a</sup> Corrected by using the atomic annihilation momentum densities.

<sup>b</sup> Corrected by using the fluorine 2p-orbital factor  $G_{\text{F},2p}(P)$ .

This suggest that if a specific atomic orbital dominates the molecular annihilation spectra, then the spectra can be brought in line with experiment using only the correction factor of this orbital.

The inclusion of the correction factors causes  $\approx 30\%$  reduction in the linewidth, as documented in table 4, and brings it into improved agreement with the measured value. Note that one can gauge the relative importance of the inclusion of the atomic potential and the inclusion of the proper vertex in fluorine by considering these effects in neon. For the valence 2s and 2p orbitals in neon, the plane-wave positron linewidth of 4.94 keV [9]. This compares with the FWHM of 3.82 keV for the HF zeroth-order-vertex calculation, and 3.55 keV, when using the Dyson orbital and full 0th + 1st-order +  $\Gamma$  vertex [6, 62]. Thus for neon the majority of the narrowing comes from the inclusion the effect of the atomic potential, and we should also expect this to be the case for  $\text{CF}_4$ . The zeroth-order HF correction factor therefore brings the calculation closer to the measured value than was observed for the corresponding quantity in  $\text{H}_2$ , where the nuclear potential is not as strong.

## 6. Summary and conclusions

Two approaches have been used to calculate  $\gamma$ -spectra for positron annihilation for a selection of molecules including methane and its fluorosubstitutes. The first method used modern quantum chemistry tools and density functional theory (B3LYP or BP86) to calculate the electron momentum densities, which were then converted into the annihilation spectra. This method assumes that a positron thermalized at room temperature can be described using the plane-wave approximation, i.e. neglecting its interaction with the target. The corresponding annihilation spectra were found to be systematically broader than experiment by about 40%.

These calculations were complemented in an approach that relied on expanding the molecular orbitals as LCAOs. It allowed us to incorporate the effect of positron-atom interactions and electron–positron correlations using momentum-dependent atomic correction factors. In particular, this method enables one to include the effect of positron-nuclear repulsion, which leads to a significant narrowing of the annihilation spectra compared to the plane-wave approximation.

For the hydrogen atoms the atomic correction factor could be calculated near exactly from many-body theory. Its inclusion produced a  $\gamma$ -spectrum of  $H_2$  in good agreement with experiment. Furthermore, for  $H_2$  the method gave the absolute annihilation rate parameter  $Z_{\text{eff}} \approx 14$  for thermal room-temperature positrons. This value is close to the commonly accepted experimental  $Z_{\text{eff}} = 14.6$  [58] and best variational calculation,  $Z_{\text{eff}} = 15.7$  [54].

For carbon and fluorine we used much simpler, Hartree–Fock positron correction factors. Nevertheless, the effective inclusion of the nuclear repulsion through these correction factors resulted in a significant narrowing of the spectra of  $CH_4$  and  $CF_4$ , giving much improved agreement with experiment. For a polyatomic molecule the annihilation spectrum is determined by contributions of many molecular orbitals. In  $CF_4$  the dominant orbitals are fluorine-2p in nature, which allows one to adjust the spectrum using a single atomic correction factor. The remaining discrepancies are due to the neglect of the positron-atom and positron–electron correlations.

Any complete *ab initio* theory of positron annihilation on molecules must include the full electron and positron dynamics, accounting for the positron–nuclear repulsion and electron–positron correlation effects. However, we have shown that realistic annihilation  $\gamma$ -spectra for molecules can be obtained from a standard LCAO electron momentum density approach, by replacing the atomic electron momentum densities with atomic annihilation momentum densities.

We have shown that the effective distortion of the electron momentum density, when it is observed through positron annihilation  $\gamma$ -spectra, can be approximated by a simple scaling which reduces the momenta and  $\gamma$ -ray Doppler shifts by a factor of 1.4. The origin of this scaling is in the similarity between the electron orbital momentum densities and corresponding momentum-dependent positron correction factors. Realistic annihilation  $\gamma$ -spectra can therefore be obtained from standard electron momentum density calculations by including this scaling. Conversely, the simple scaling factor allows for the deduction of electron momentum densities from positron annihilation  $\gamma$ -spectra.

## Acknowledgments

We thank Eric Spencer for assistance in comparisons of the quantum chemical predictions and experimental data for molecular annihilation spectra. DGG was funded by a DEL Northern

Ireland postgraduate studentship. FW and SS acknowledge the support of the Australian Research Council under the Discovery Project scheme, and the National Computational Infrastructure at the Australian National University under the Merit Allocation Scheme. The research at the University of California, San Diego is supported by the NSF, Grant no. PHY 10-68023.

## References

- [1] Dirac P A M 1930 *Math. Proc. Camb. Phil. Soc.* **26** 361
- [2] Berestetskii V B, Lifshitz E M and Pitaevskii L P 1982 *Quantum Electrodynamics (Course of Theoretical Physics vol 4)* 2nd edn (Oxford: Pergamon)
- [3] Iwata K, Greaves R G and Surko C M 1997 *Phys. Rev. A* **55** 3586
- [4] Iwata K, Gribakin G F, Greaves R G and Surko C M 1997 *Phys. Rev. Lett.* **79** 39
- [5] Reeth P V, Humberston J W, Iwata K, Greaves R G and Surko C M 1996 *J. Phys. B: At. Mol. Phys.* **29** L465
- [6] Dunlop L J M and Gribakin G F 2006 *J. Phys. B: At. Mol. Opt. Phys.* **39** 1647
- [7] Green D G and Gribakin G F 2012 Positron scattering and annihilation on hydrogen-like ions, unpublished
- [8] Green D G and Gribakin G F 2012 Enhancement and spectra of positron annihilation on core and valence electrons, unpublished
- [9] Wang F, Selvam L, Gribakin G F and Surko C M 2010 *J. Phys. B: At. Mol. Opt. Phys.* **43** 165207
- [10] Schultz P J and Lynn K G 1988 *Rev. Mod. Phys.* **60** 701
- [11] Puska M J and Nieminen R M 1994 *Rev. Mod. Phys.* **66** 841
- [12] Saniz R, Barbiellini B and Denison A 2002 *Phys. Rev. B* **65** 245310
- [13] Weber M H, Lynn K G, Barbiellini B, Sterne P A and Denison A B 2002 *Phys. Rev. B* **66** 041305
- [14] Saniz R, Barbiellini B, Denison A B and Bansil A 2003 *Phys. Rev. B* **68** 165326
- [15] Eijt S W H, van Veen A, Schut H, Mijnarends P E, Denison A B, Barbiellini B and Bansil A 2006 *Nature Mater.* **5** 23
- [16] Eijt S W H, Mijnarends P E, van Schaarenburg L C, Houtepen A J, Vanmaekelbergh D, Barbiellini B and Bansil A 2009 *Appl. Phys. Lett.* **94** 091908
- [17] Meng X Q, Chen Z Q, Jin P, Wang Z G and Wei L 2007 *Appl. Phys. Lett.* **91** 093510
- [18] Nagai Y, Toyama T, Tang Z, Inoue K, Chiba T, Hasegawa M, Hirosawa S and Sato T 2009 *Phys. Rev. B* **79** 201405
- [19] Maekawa M, Kawasuso A, Yoshikawa M, Miyashita A, Suzuki R and Ohdaira T 2006 *Phys. Rev. B* **73** 014111
- [20] Eijt S W H, Barbiellini B, Houtepen A J, Vanmaekelbergh D, Mijnarends P E and Bansil A 2007 *Phys. Status Solidi c* **4** 3883
- [21] Asoka-Kumar P, Alatalo M, Ghosh V J, Kruseman A C, Nielsen B and Lynn K G 1996 *Phys. Rev. Lett.* **77** 2097
- [22] Petkov M P, Weber M H, Lynn K G, Crandal I R S and Ghosh V J 1999 *Phys. Rev. Lett.* **82** 3819
- [23] Alatalo M, Kauppinen H, Saarinen K, Puska M J, Mäkinen J, Hautojärvi P and Nieminen R M 1995 *Phys. Rev. B* **51** 4176
- [24] Kim S, Eshed A, Goktepeli S, Sterne P A, Koymen A R, Chen W C and Weiss A H 2006 *Phys. Rev. B* **73** 014114
- [25] Mayer J, Schreckenbach K and Hugenschmidt C 2007 *Phys. Status Solidi c* **4** 3928
- [26] Gribakin G F, Young J A and Surko C M 2010 *Rev. Mod. Phys.* **82** 2557
- [27] Brown B L and Leventhal M 1986 *Phys. Rev. Lett.* **57** 1651
- [28] Tang S, Tinkle M D, Greaves R G and Surko C M 1992 *Phys. Rev. Lett.* **68** 3793
- [29] Armour E A G and Carr J M 1997 *J. Phys. B: At. Mol. Phys.* **30** 1611
- [30] Darewych J W 1979 *Can. J. Phys.* **57** 1027
- [31] Ghosh A S, Mukherjee T and Darewych J W 1994 *Hyperfine Interact.* **89** 319
- [32] Chuang S Y and Hogg B G 1967 *Can. J. Phys.* **45** 3895

- [33] Wang F, Ma X, Selvam L, Gribakin G and Surko C M 2012 Chemical structural effects on  $\gamma$ -ray spectra of positron annihilation in fluorobenzenes *Eur. Phys. J. D* at press
- [34] Green D G, Saha S, Wang F, Gribakin G F and Surko C M 2011 *Mater. Sci. Forum* **666** 21
- [35] Akhiezer A I and Berestetskii V B 1982 *Quantum Electrodynamics* (New York: Interscience)
- [36] Gribakin G F and Ludlow J 2004 *Phys. Rev. A* **70** 032720
- [37] Gribakin G F and Ludlow J 2002 *J. Phys. B: At. Mol. Opt. Phys.* **35** 339
- [38] McCarthy I E and Weigold E 1991 *Rep. Prog. Phys.* **54** 789
- [39] Fraser P A 1968 *Adv. At. Mol. Phys.* **4** 63
- [40] Pomeranchuk I 1949 *Zh. Eksp. Teor. Fiz.* **19** 183
- [41] Becke A D 1993 *J. Chem. Phys.* **98** 5648
- [42] Lee C, Yang W and Parr R G 1988 *Phys. Rev. B* **37** 785
- [43] Godbout N and Salhub D R 1992 *Can. J. Chem.* **70** 560
- [44] Wang F 2003 *J. Phys. Chem. A* **107** 10199
- [45] Gaussian M J and Frisch *et al* 2004 *Gaussian 03* (Wallingford, CT: Gaussian, Inc)
- [46] Schmidt M W *et al* 1993 *J. Comput. Chem.* **14** 1347
- [47] Kajser P and Jr V H S 1977 *Adv. Quantum Chem.* **10** 37
- [48] Varshalovich D A, Moskalev A N and Khersonskii V K 1988 *Quantum Theory of Angular Momentum* (Singapore: World Scientific)
- [49] Slater J C 1963 *Quantum Theory of Molecules and Solids* (New York: McGraw-Hill)
- [50] Green D G 2011 Positron annihilation with core electrons *PhD Thesis* Queen's University, Belfast
- [51] Armour E A G and Baker D J 1986 *J. Phys. B: At. Mol. Phys.* **19** L871
- [52] Cooper J N, Armour E A G and Plummer M 2008 *J. Phys. B: At. Mol. Opt. Phys.* **41** 245201
- [53] Armour E A G, Cooper J N, Gregory M R, Jonsell S, Plummer M and Todd A C 2010 *J. Phys.: Conf. Ser.* **199** 012007
- [54] Zhang J Y, Mitroy J and Varga K 2009 *Phys. Rev. Lett.* **103** 223202
- [55] Zhang R, Baluja K L, Franz J and Tennyson J 2011 *J. Phys. B: At. Mol. Opt. Phys.* **44** 035203
- [56] McNutt J D, Sharma S C and Brisbon R D 1979 *Phys. Rev. A* **20** 347
- [57] Wright G L, Charlton M, Clark G, Griffith T C and Heyland G R 1983 *J. Phys. B: At. Mol. Opt. Phys.* **16** 4065
- [58] Laricchia G, Charlton M, Beling C D and Griffith T C 1987 *J. Phys. B: At. Mol. Phys.* **20** 1865
- [59] Cotton F A 1990 *Chemical Applications of Group Theory* 3rd edn (New York: Wiley-Interscience)
- [60] Pitzer R M 1967 *J. Chem. Phys.* **46** 4871
- [61] Rozenberg E L and Dyatkina M E 1971 *J. Struct. Chem.* **12** 270
- [62] Dunlop L J M 2005 Theory of positron–atom annihilation gamma spectra *PhD Thesis* Queen's University, Belfast